Look-Ahead Cyclic Pitch Control Using LIDAR

David Schlipf[1] Simone Schuler[2] Patrick Grau[2] Frank Allgöwer[2] Martin Kühn[1*]

[1]Endowed Chair of Windenergy
Universität Stuttgart
Allmandring 5B, D-70569 Stuttgart
schlipf@ifb.uni-stuttgart.de

[2]Institute for Systems Theory and Automatic Control
Universität Stuttgart
Pfaffenwaldring 9, D-70550 Stuttgart
schuler, allgower@ist.uni-stuttgart.de

Abstract

LIDAR (Light detection and ranging) systems are able to provide preview information of wind disturbances at various distances in front of wind turbines. This information can be used to improve the control of wind turbines. This paper compares a predictive feedforward control structure combined with common PI controllers to a baseline controller and to an $\mathcal{H}_\infty$ approach showing the advantage of look-ahead control to reduce wind turbine loads. The control design is verified by simulations with a turbulent wind field and a full nonlinear model of the wind turbine.

Keywords: wind turbine, load reduction, cyclic pitch, disturbance compensation, look-ahead control, $\mathcal{H}_\infty$-optimal control, LIDAR assisted control

1 Introduction

Reducing loads by control is an important issue for wind energy since atmospheric turbulence produces fatigue and extreme loads which are the main design driver for large wind turbines. But in terms of control theory, transients such as gusts, varying shears and directional changes in the inflow wind field represent an unknown disturbance. Conventional feedback controllers can compensate such excitations only with a delay since the disturbance has to pass the entire wind turbine dynamics before showing its effects in the outputs and since the actuators need time to react. This usually results in undesired loads for the wind turbine and high actuator rates.

In [1] it has been shown that loads and pitch rates can be reduced significantly with a predictive feedforward control strategy as an extension to a common collective pitch controller, assuming perfect measurements of the inflow wind field and using Taylor's frozen turbulence hypothesis. But the collective pitch control cannot compensate for the asymmetric loads caused by vertical or horizontal wind shear. In [2] an $\mathcal{H}_\infty$ preview feedforward control assuming highly idealized, rotating wind measurements shows significant improvements in load mitigation with reasonable pitch rates. However, the results using wind measurements in three stationary points show that without further optimization the advantage, compared to a controller based only on turbine feedback, disappears.

This work illustrates that the improvement by the knowledge of future inflow wind fields still persists if a simple and robust control strategy is used combined with realistic simulation of LIDAR measurements. Here, the look-ahead control introduced in [1] is extended to cyclic pitch control with common PI controllers as presented in [3] and compared with a baseline controller and an $\mathcal{H}_\infty$ approach to estimate the advantage of look-ahead control to reduce wind turbine loads. Furthermore some effort has been undertaken to reduce the complex disturbance to useable wind characteristics and extract them realistically from a wind field by simulating inflow measurements with LIDAR.

This paper is organized as follows: Section 2 deals with the modeling of the wind inflow and turbine. Section 3 describes the simulated LIDAR measurements and in Section 4 different controllers were designed. Simulation results with the full nonlinear model and a full-field stochastic wind are shown in Section 5 and Section 6 concludes the paper.

2 Modeling of Wind Disturbance and Turbine

Wind turbines are normally simulated with aeroelastic models and achieve good correlation with reality [4]. The wind disturbance is generally a stochastic vector field in a Cartesian or polar grid. But complex turbine models with these multi-dimensional

*now at ForWind - University of Oldenburg
martin.kuehn@uni-oldenburg.de

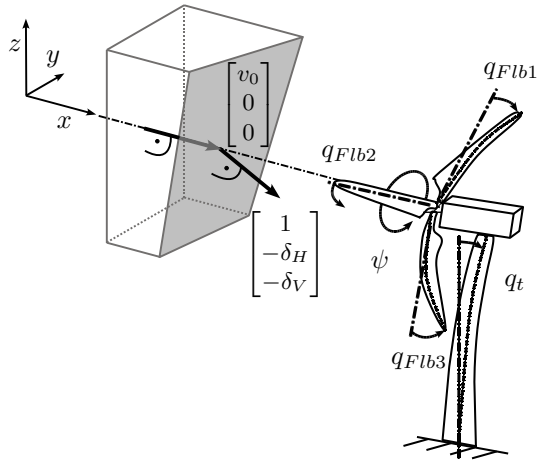

Figure 1: Reduced wind disturbance and considered modes of a wind turbine.

disturbance inputs are unsuitable for controller design. The challenge of this section is to reduce the wind disturbance and wind turbine to simpler models which can be used for controller design, but still result in controllers that can be successfully evaluated with a full aeroelastic model and turbulent wind fields.

2.1 Modeling of the Wind Disturbance

The turbulent wind disturbance (see Figure 1) is reduced to the disturbances vector d_{0HV}, which is defined as follows

$$d_{0HV} = \begin{bmatrix} v_0 & \delta_H & \delta_V \end{bmatrix}^T,$$

where v_0 is the horizontal hub-height wind speed and δ_H and δ_V are the horizontal and vertical shear, respectively. Thus the wind input vector v_{wind} depends on its horizontal and vertical position (y,z):

$$v_{wind}(y,z) = \begin{bmatrix} v_0 + \delta_H y + \delta_V z \\ 0 \\ 0 \end{bmatrix}. \qquad (1)$$

By this spatial turbulence and misalignment of the turbine are neglected, but d_{0HV} can be used for feedforward control.

2.2 The nonlinear model

The $\mathcal{H}_\infty$-optimal individual pitch control needs a linear time-invariant (LTI) design model including the most relevant modes for the control problem. The LTI model is derived from an azimuth dependent nonlinear model considering the rotor motion, first flapwise bending modes of each blade and the first tower fore-aft bending mode as depicted in Figure 1.
The nonlinear aeroelastic equations of motion for the modeled wind turbine with the above mentioned modes can be written as follows (see [5])

$$M(q,u,t)\,\ddot{q} + f(q,\dot{q},u,d_{0HV},t) = 0$$
$$y = h(q,\dot{q},t), \qquad (2)$$

where f and h are nonlinear function vectors, M is the mass matrix, t is time, and q is the vector of the considered tower fore-aft bending mode q_T, rotor azimuth angle ψ and flapwise bending modes q_{Flbi} of each blade:

$$q = \begin{bmatrix} q_T & \psi & q_{Flb1} & q_{Flb2} & q_{Flb3} \end{bmatrix}^T.$$

The disturbances vector d_{0HV} is modeled as described in Section 2.1 and the control inputs u are the pitch angles θ_i of each blade:

$$u = \begin{bmatrix} \theta_1 & \theta_2 & \theta_3 \end{bmatrix}^T.$$

The considered outputs are the rotor speed $\dot{\psi}$ and the flapwise bending moments of each blade M_{Flbi}:

$$y = \begin{bmatrix} \dot{\psi} & M_{Flb1} & M_{Flb2} & M_{Flb3} \end{bmatrix}^T.$$

Compared to the more complex model of Section 5 only five modes are modeled out of 19.

2.3 The decoupled LTI model

A linear time-invariant (LTI) model is obtained by linearization of (2) and a multi-blade coordinate transformation on the periodic wind turbine model (see Figure 2 and [6]).

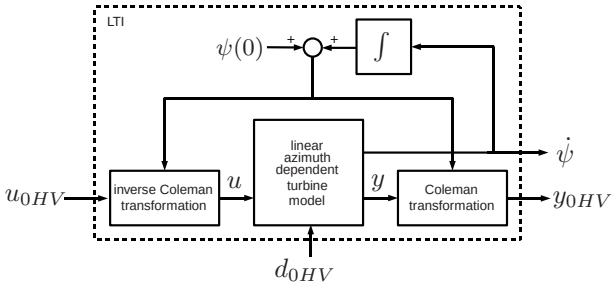

Figure 2: LTI system.

With further simplifications (see [7]) this system can be decoupled:

$$\begin{bmatrix} M_0 & 0 \\ 0 & M_{HV} \end{bmatrix} \ddot{q}_{0HV} + \begin{bmatrix} D_0 & 0 \\ 0 & D_{HV} \end{bmatrix} \dot{q}_{0HV} + \begin{bmatrix} S_0 & 0 \\ 0 & S_{HV} \end{bmatrix}$$
$$q_{0HV} = \begin{bmatrix} F_0 & 0 \\ 0 & F_{HV} \end{bmatrix} u_{0HV} + \begin{bmatrix} F_{d0} & 0 \\ 0 & F_{dHV} \end{bmatrix} d_{0HV}$$
$$y_{0HV} = \begin{bmatrix} C_{v0} & 0 \\ 0 & C_{vHV} \end{bmatrix} \dot{q}_{0HV} + \begin{bmatrix} C_{d0} & 0 \\ 0 & C_{dHV} \end{bmatrix} q_{0HV}, \qquad (3)$$

where D is the damping, S the stiffness, F the control input, F_d the wind input, C_v the velocity output and C_d the displacement output matrix denoted with 0 referring to the horizontal hub-height wind speed and H and V referring to the horizontal and vertical wind shear.
The matrices of the HV subsystem can be organized in the usual state space representation

$$\begin{aligned} \dot{x}_{HV} &= Ax_{HV} + B_1 d_{HV} + B_2 u_{HV} \\ y_{HV} &= C_2 x_{HV} + D_{21} d_{HV} + D_{22} u_{HV}, \end{aligned} \qquad (4)$$

where the state vector is $x_{HV} = \begin{bmatrix} q_{HV} & \dot{q}_{HV} \end{bmatrix}^T$. The model is stable with minimum-phase behavior.

3 Simulated LIDAR measurements

In Section 2.1 the complex wind field disturbance has been reduced to a horizontal wind speed at hub height and horizontal and vertical shear. To get a more realistic estimate from the frequency domain in which these wind characteristics can be predicted, measurements are simulated with the LIDAR simulator presented in [8]. A circle is swept in $2.4\ \mathrm{s}$ with 12 points in each of five different distances and was chosen for the trajectory (see Figure 3).

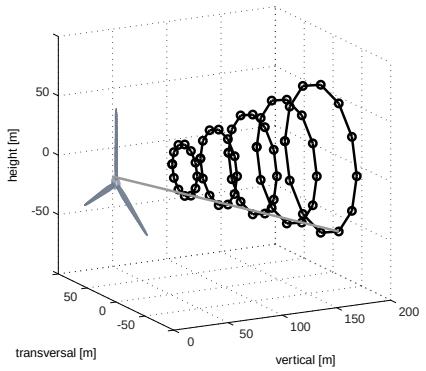

Figure 3: Scope of nacelle based pulsed LIDAR measurements.

This trajectory was realized by the LIDAR system developed by the SWE installed on the nacelle of a $5\ \mathrm{MW}$ turbine [9]. In the simulation, effects as collision of the laser with the blades, volume measurement and mechanical constrains of the scanner from data of the real experiment are considered to obtain realistic measurements. For instance the same loss of circa 30% points could be observed in the simulation and in the measurements due to the collision with moving blades.
Taylor's frozen turbulence is assumed, both in the simulation of the measurements and the wind field reconstruction. As LIDAR systems measure only the wind speed in line-of-sight direction, the 3D wind vector is reconstructed using the assumption of perfect alignment with the wind. From the simulated measurements, d_{0HV} is obtained online with least squares methods over the last 12 measurements and equation (1). Figure 4 shows the coherence between the effective wind speed from the simulated and perfect measurements. A good correlation can be observed for frequencies below $0.1\ \mathrm{Hz}$ and therefore the signals for the feed-forward control update are filtered by a low pass filter (2nd order, cut-off frequency $0.1\ \mathrm{Hz}$) to avoid incorrect control action caused by inaccurate predictions. It is also convenient to filter out frequencies above $0.1\ \mathrm{Hz}$ because of the validated frequency domain of Taylor's frozen turbulence theorem ([10],[11]).

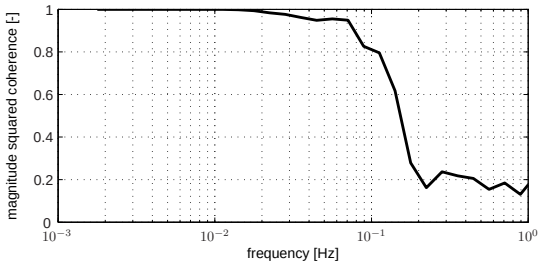

Figure 4: Coherence between the simulated and perfect LIDAR measurements.

4 Controller Design

The used control structure is depicted in Figure 5.

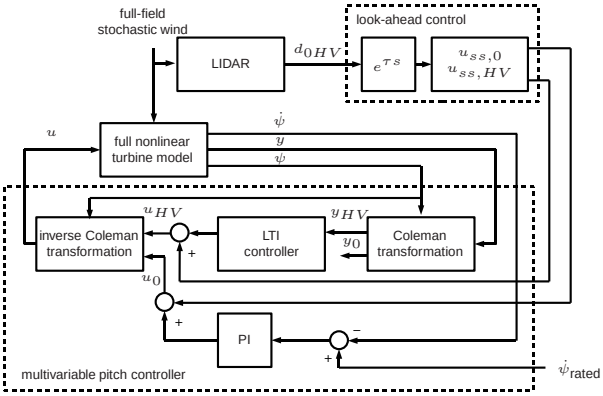

Figure 5: Closed loop for cyclic pitch control: LTI controller either represents an $\mathcal{H}_\infty$ or two PI controller, if look-ahead control is used.

The baseline PI controller controls the rotor speed $\dot{\psi}$. The turbine is operated above rated wind

condition and the torque controller maintains constant power. The second controller combines the baseline PI with an $\mathcal{H}_\infty$ controller for the H and V feedback part to minimize the blade root bending moment. The third option is the baseline controller with two PI controllers for the H and V part and a look-ahead extension for all three.

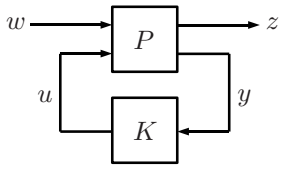

Figure 6: PK-structure used for $\mathcal{H}_\infty$-control design.

4.1 Baseline controller

The baseline controller is implemented based on [12]: To mitigate high-frequency excitation of the control systems, the rotor speed measurement is filtered for all controllers using a single-pole low-pass filter with a corner frequency of $0.25\ \mathrm{Hz}$. Then the collective blade pitch angle command is computed using a gain-scheduled PI controller on the speed error between the filtered and the rated rotor speed.

4.2 $\mathcal{H}_\infty$ controller

Linear time-invariant (LTI) multi-input/multi-output (MIMO) systems P with state space descriptions

$$\begin{bmatrix} \dot{x}(t) \\ z(t) \\ y(t) \end{bmatrix} = \begin{bmatrix} A & B_1 & B_2 \\ C_1 & D_{11} & D_{12} \\ C_2 & D_{21} & D_{22} \end{bmatrix} \begin{bmatrix} x(t) \\ w(t) \\ u(t) \end{bmatrix} \tag{5}$$

are considered, to find an $\mathcal{H}_\infty$-controller K (see Figure 6), where the variables denote states $x \in \mathbb{R}^n$, reference signal and exogenous disturbance $w \in \mathbb{R}^{q_1}$, control inputs $u \in \mathbb{R}^{q_2}$, performance outputs $z \in \mathbb{R}^{p_1}$ and measurements $y \in \mathbb{R}^{p_2}$. This description may include static or dynamic weighting factors. Assumptions on the system are stabilizability of (A, B_2) and detectability of (A, C_2). The exogenous disturbances are allowed to be elements of $\mathcal{L}_2^{q_1}$, which is the Hilbert space of right-sided square integral signals $s(t)$ with the norm

$$\|s\|_{\mathcal{L}_2} = \sqrt{\int_0^\infty s(t)^T s(t) dt}$$

This means that the signals are of finite energy. The $\mathcal{L}_2$-induced norm or energy gain between exogenous inputs w and performance outputs z of the system operator $T : \mathcal{L}_2^{q_1} \to \mathcal{L}_2^{p_1}$ is defined as

$$\|T\|_{\mathcal{L}_2 - ind} := \sup_{0 \le w \le \infty} \frac{\|Tw\|_{\mathcal{L}_2}}{\|w\|_{\mathcal{L}_2}}.$$

For an LTI operator or transfer function, the $\mathcal{L}_2$-induced norm is equivalent to the maximum singular value $\bar{\sigma}$ of the transfer function of the system, which is the systems $\mathcal{H}_\infty$-norm [13]. The goal for $\mathcal{H}_\infty$ controller design is to find a controller K that internally stabilizes the closed loop and minimizes its $\mathcal{H}_\infty$-gain from external disturbance signals w (i.e. wind) to the desired performance output z (i.e. blade root bending moment). The usefulness of the $\mathcal{H}_\infty$-approach results from the possibility of closed loop shaping. Desired closed loop properties, such as no steady state error, bandwidth or robustness, can be directly considered. Dynamical $\mathcal{H}_\infty$-output feedback controllers can be efficiently computed via semi-definite programming and standard solvers [14]. The individual pitch $\mathcal{H}_\infty$ controller should compensate the horizontal and vertical blade root bending moments and guarantee robustness in face of uncertainties in the aeroelastic coefficients. To design such a controller for the model given in (4), a classical mixed sensitivity approach is used with weighting functions to shape the sensitivity S and to penalize the control signal

$$\left\| \begin{matrix} W_S S \\ W_{KS} K S \end{matrix} \right\|_\infty \le 1,$$

where the inverse of W_S and W_{KS} exhibit the desired shape, respectively upper bounds of S and KS. The resulting stable $\mathcal{H}_\infty$ controller has an order of $n = 6$.

4.3 Look-ahead controller

The block diagram in Figure 7 illustrates the used look-ahead control schema for a general control problem.

Here the output y of the system Σ is influenced by two signals: the control input u and the disturbance d. Then the system Σ can be divided into two subsystems, Σ_{yu} and Σ_{yd}. In a basic control loop - if no feedforward is used - the feedback controller Σ_{FB} is responsible for reference signal tracking and disturbance rejection.

If d is forwarded by Σ_{FF} and added to the feedback controller output u_{FB}, theoretically a perfect compensation of the disturbance can be reached with $\Sigma_{FF} = -\Sigma_{yu}^{-1}\Sigma_{yd}$. In this case the feedback controller Σ_{FB} is responsible for reference signal tracking only and Σ_{FF} for disturbance compensation. For the pitch control problem this separation is convenient, because the control task is to compensate the wind disturbance and the reference signals are constant.

In practice, the perfect compensation can often not be achieved or is not robust due to model uncertainties as in the case of the nonlinear wind turbine

model.
Therefore, in [1] a static compensation was proposed

$$\underset{t\to\infty}{\Sigma_{FF}} = u_{ss}(d_{ss}),$$

which is the static value u_{ss} of the system input subject to the static disturbance d_{ss}. The static compensation is combined with a prediction: the disturbance d is applied in advance by the prediction time shift τ. The appropriate prediction time τ depends on the difference in the relative degrees of Σ_{yd} and Σ_{yu}. Stability of the control loop is neither influenced by the added static feed-forward control nor by the time shift, because none of the newly implemented blocks is part of the closed control loop and no additional poles were introduced [15].
In the case of pitch control, Σ_{yu} has a higher relative degree, because pitch angles have a delayed impact on the rotor speed compared to the wind disturbance due to the pitch actuator dynamics. Therefore a prediction time τ shifts the disturbance signal in time in such a way that the pitch moves earlier. In the presented case a time shift of $0.7\ \mathrm{s}$ was used to overcome the pitch dynamics. Due to the LIDAR measurement in front of the rotor plane this prediction is possible.
The static functions for the feedforward part of the look-ahead controller can be obtained from simulations or from modeling.
For the asynchronous part, (3) is used with $\dot{x}_{HV} = 0$ and $y_{HV} = 0$, because the feed-forward input $u_{FF,HV}$ is designed to compensate influences from d_{HV} to y_{HV} in the steady state. The same idea is used in the disturbance accommodating control (DAC) proposed in [16]. As the system is strictly proper and due to the simplifications, the following relation is obtained where the $(*)^+$ symbol indicates the application of the Moore-Penrose pseudoinverse:

$$u_{ss,HV} = -B_2^+ B_1 d_{ss,HV} = \begin{bmatrix} g_H & 0 \\ 0 & g_V \end{bmatrix} d_{ss,HV}. \quad (6)$$

For the synchronous part, the nonlinear function $u_{ss,0}(d_{ss,0})$ of the static collective pitch over static wind speed is used. This function can be obtained by simulation with the nonlinear model and is documented in [12].
Altogether only the two gains g_H and g_V, the prediction time τ and the static collective pitch over static wind speed $u_{ss,0}(d_{ss,0})$ are needed to implement the proposed look-ahead control as an update to a existing PI control structure. The advantage of this simplicity is that in a real application these requirements could be adjusted online, e.g. τ could be obtained by a cross-correlation of LIDAR measurement and a wind estimate from turbine data.

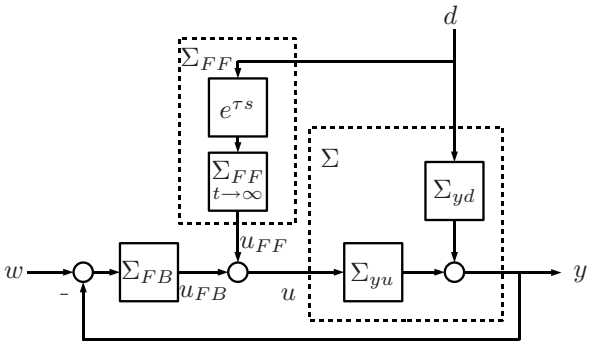

Figure 7: General control loop with look ahead control for disturbance compensation.

5 Simulation Results

Simulations are done with a stochastic full-field wind (23×23 grid, $\Delta t = 0.25\ \mathrm{s}$) with mean velocity $16\ \mathrm{m/s}$ and turbulence intensity of 18% and the nonlinear model combined with the above described controllers as depicted in Figure 8. The model as given in [12] was extended with individual pitch actuator dynamics (second order linear model, pitch rate limited to $8°/\mathrm{s}$). Notch filters (butterworth, 2nd order) with stop band $[0.9f_j, 1.1f_j]$ are used, where f_j is the 2P and 4P frequency, respectively. The phase shift through pitch actuator and filters is considered in the Coleman transformation. For the look-ahead controller the simulation was coupled with the LIDAR simulator [8] to obtain realistic measurements during the simulation.
It can be seen, that both the $\mathcal{H}_\infty$ controller and the look-ahead controller stabilize the nonlinear system and lead to satisfying control performance, decreasing the blade bending moment significantly in comparison to the usual baseline controller, at the expense of an increased input signal. Standard deviation of several signals are shown in Table 1.

	baseline	$\mathcal{H}_\infty$	look-ahead
$\sigma(M_{oop1})/[\mathrm{MNm}]$	1.93	1.65	1.39
$\sigma(M_{yT})/[\mathrm{MNm}]$	12.1	12.6	10.7
$\sigma(\dot{\psi})/[rpm]$	0.25	0.25	0.12
$\sigma(\dot{\theta}_1)/[°/\mathrm{s}]$	0.68	2.56	1.86

Table 1: Standard deviations from the simulation.

Results are more obvious in the frequency domain, see Figure 9. Both controllers reduce the blade bending moment near the 1P-frequency ($\approx 0.2\ \mathrm{Hz}$), but only the look-ahead controller can significantly reduce loads on tower and blades below the 1P-frequency due to the feedforward control. The look-ahead controller needs a higher pitch rate near the 1P frequency, the $\mathcal{H}_\infty$ over a broader band.

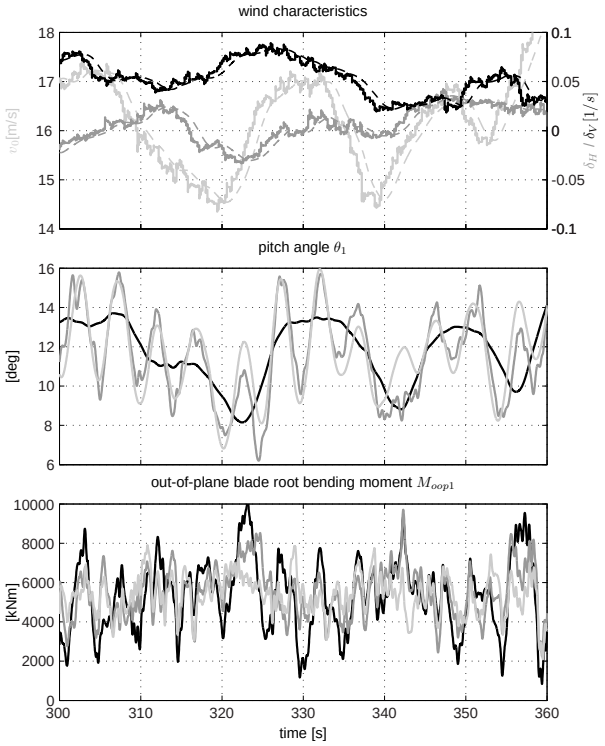

Figure 8: Simulation for a turbulent wind field for the baseline (black), the $\mathcal{H}_\infty$ (dark gray) and the look-ahead controller (light gray). The simulated LIDAR measurements are solid (v_0 light gray, δ_H dark gray, δ_V black), the filtered data dashed.

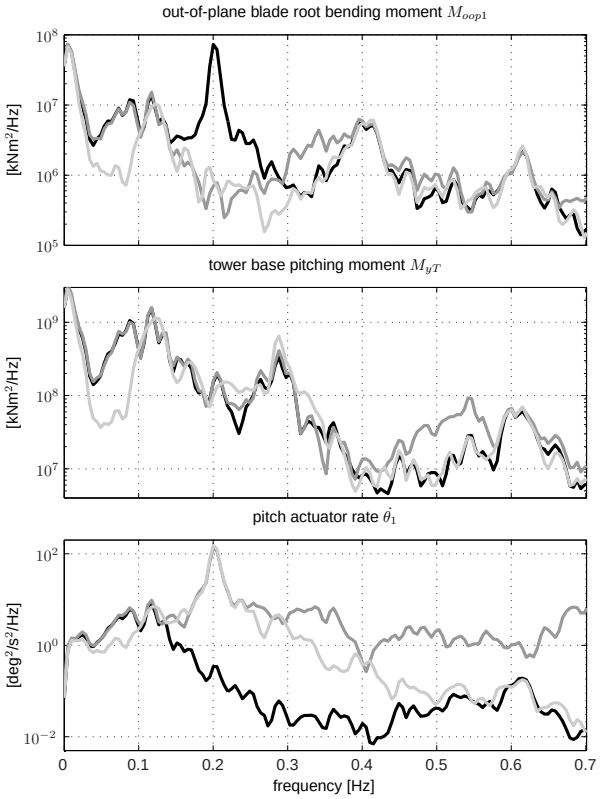

Figure 9: Power spectral densities for the baseline (black), the $\mathcal{H}_\infty$ (dark gray) and the look-ahead controller (light gray).

6 Conclusion and Outlook

In this paper a look-ahead cyclic pitch control based on LIDAR wind field measurement has been presented. A first evaluation with simulated measurements of a real LIDAR system has been given through a comparison to a baseline and an $\mathcal{H}_\infty$ cyclic pitch controller. Load reduction on blades and tower can be achieved by extending common PI controllers with a predictive feedforward update. The pitch dynamics are moderate compared to the presented $\mathcal{H}_\infty$ approach. The proposed structure relies on few variables which can easily be obtained from simulations or data analysis.
In further studies a more detailed load analysis will be performed. For a better comparison, the baseline will be combined with a active tower damping. The wind model has to be extended by a wind direction to compensate the effects of wind direction changes not yet considered.

7 Acknowledgment

Part of this research is funded by the German Federal Ministry for the Environment, Nature Conservation and Nuclear Safety (BMU) in the framework of the German joint research project ”Development of LIDAR technologies for the German offshore test field”.

References

[1] Schlipf, D. and Kühn, M., “Prospects of a Collective Pitch Control by Means of Predictive Disturbance Compensation Assisted by Wind Speed Measurements,” *Proc. DEWEK* , 2008.

[2] Laks, J., Pao, L. Y., Wright, A., Kelley, N., and Jonkman, B., “Blade Pitch Control with Preview Wind Measurements,” *Proc. 48th AIAA Aerospace Sciences Meeting Including the New Horizons Forum and Aerospace Exposition*, 2010.

[3] Bossanyi, E. A., “Wind Turbine Control for Load Reduction,” *Wind Energy*, Vol. 6, 2003, pp. 229–244.

[4] Rossetti, M., “Wind turbine dynamics validation and controller optimisation,” *Proc. EWEC*, 2008.

[5] Jonkman, J. and Buhl, M., “FAST User’s Guide,” 2005.

[6] Schuler, S., Schlipf, D., Kühn, M., and Allgöwer, F., “ℓ_1-Optimal Multivariable Pitch Control for Load Reduction on Large Wind Turbines,” *Proc. EWEC*, 2010.

[7] Geyler, M. and Caselitz, P., “Robust Multivariable Pitch Control Design for Load Reduction on Large Wind Turbines,” *ASME Journal of Solar Energy Engineering*, Vol. 130, 2008.

[8] Schlipf, D., Trujillo, J. J., Basterra, V., and Kühn, M., “Development of a Wind Turbine LIDAR Simulator,” *Proc. EWEC*, 2009.

[9] Rettenmeier, A., Bischoff, O., Hofsäss, M., Schlipf, D., Trujillo, J. J., and Kühn, M., “Wind field analyses using a nacelle-based LIDAR system,” *Proc. EWEC*, 2010.

[10] Sjöholm, M., Mikkelsen, T., Kristensen, L., Mann, J., Kirkegaarda, P., Kapp, S., Schlipf, D., and Trujillo, J. J., “Spectral analysis of wind turbulence measured by a Doppler LIDAR for velocity fine structure and coherence studies,” *Proc. ISARS*, 2010.

[11] Schlipf, D., Trabucchi, D., Bischoff, O., Hofsäss, M., Mann, J., Mikkelsen, T., Rettenmeier, A., Trujillo, J. J., and Kühn, M., “Testing of Frozen Turbulence Hypothesis for Wind Turbine Applications with a Scanning LIDAR System,” *Proc. ISARS*, 2010.

[12] Jonkman, J., Butterfield, S., Musial, W., and Scott, G., “Definition of a 5-MW reference wind turbine for offshore system development,” 2007.

[13] Zhou, K., Doyle, J. C., and Glover, K., *Robust and Optimal Control*, Upper Saddle River, NJ: Prentice Hall, 1996.

[14] Gahinet, P. and Apkarian, P., “A linear matrix inequality approach to $\mathcal{H}_\infty$ control,” *Int. J. Robust and Nonlinear Control*, Vol. 4, 1994, pp. 421–448.

[15] Graichen, K., Hagenmeyer, V., and Zeitz, M., “A new approach to inversion-based feedforward control design for nonlinear systems,” *Automatica*, Vol. 41, 2005, pp. 20332041.

[16] Namik, H. and Stol, K., “Individual Blade Pitch Control of a Floating Offshore Wind Turbine on a Tension Leg Platform,” *Proc. 48th AIAA Aerospace Sciences Meeting Including the New Horizons Forum and Aerospace Exposition*, 2010.